**Annales
Geophysicae**

Rotational temperature of N_2^+ (0,2) ions from spectrographic measurements used to infer the energy of precipitation in different auroral forms and compared with radar measurements

O. Jokiaho[1], B. S. Lanchester[1], N. Ivchenko[2], G. J. Daniell[1], L. C. H. Miller[1], and D. Lummerzheim[3]

[1]School of Physics and Astronomy, University of Southampton, UK
[2]Space and Plasma Physics, School of Electrical Engineering, KTH, Stockholm, Sweden
[3]Geophysical Institute, University of Alaska, Fairbanks, AK, USA

Abstract. High resolution spectral data are used to estimate neutral temperatures at auroral heights. The data are from the High Throughput Imaging Echelle Spectrograph (HiTIES) which forms part of the Spectrographic Imaging Facility (SIF), located at Longyearbyen, Svalbard in Norway. The platform also contains photometers and a narrow angle auroral imager. Quantum molecular spectroscopy is used for modelling N_2^+ 1NG (0,2), which serves as a diagnostic tool for neutral temperature and emission height variations. The theoretical spectra are convolved with the instrument function and fitted to measured rotational transition lines as a function of temperature. Measurements were made in the magnetic zenith, and along a meridian slit centred on the magnetic zenith. In the results described, the high spectral resolution of the data (0.08 nm) allows an error analysis to be performed more thoroughly than previous findings, with particular attention paid to the correct subtraction of background, and to precise wavelength calibration. Supporting measurements were made with the Svalbard Eiscat Radar (ESR). Estimates were made from both optical and radar observations of the average energy of precipitating electrons in different types of aurora. These provide confirmation that the spectral results are in agreement with the variations observed in radar profiles. In rayed aurora the neutral temperature was highest (800 K) and the energy lowest (1 keV). In a bright curling arc, the temperature at the lower border was about 550 K, corresponding to energies of 2 keV. The radar and modelling results confirm that these average values are a lower limit for an estimation of the characteristic energy. In each event the energy distribution is clearly made up of more than one spectral shape. This work emphasises the need for high time resolution as well as high spectral resolution. The present work is the first to provide rotational temperatures using a method which pays particular attention to errors in measurement and fitting, and background subtraction.

Keywords. Atmospheric composition and structure (Airglow and aurora) – Ionosphere (Auroral ionosphere; Instruments and techniques)

1 Introduction

It has been recognised for more than half a century that spectral measurements of the rotational molecular bands of emitting species in the upper atmosphere can be used to deduce the temperature of the neutral atmosphere. In order to do this it is assumed that the emitting species are in thermal equilibrium with their local environment. If the height profile of the atmospheric temperature is known or modelled, this process can be reversed to provide the height of the emitting species and hence the energy of the precipitating electrons.

In the study of aurora, observing the temporal and spatial changes in the energy distribution of the incoming particles is key to understanding the source regions of these energetic particles. The advent of charge coupled device (CCD) detectors in the field of spectroscopy has provided the means to increase sensitivity as well as resolution in wavelength and time. Imaging spectrographs are currently the optimal instruments for high spectral resolution measurements of auroral signatures. Such measurements allow us to build on techniques that were well understood in the 1950s, and obtain more accurate estimates of the physical processes.

Koehler et al. (1981) provide a comprehensive description of the first measurements of rotational temperatures of emitting N_2^+ ions, and the subsequent application of these results to auroral physics. These early publications include Vegard (1932); Harang (1951); Shepherd and Hunten (1955); Hunten et al. (1963); Brandy (1964); Hilliard and Shepherd

Correspondence to: O. Jokiaho
(opj100@phys.soton.ac.uk)

(1966); Miller and Shepherd (1968); Zwick and Shepherd (1973); Shepherd and Eather (1976). Once the atmospheric temperature profile was established, following satellite measurements and modelling studies (Hedin, 1991), it became clear that spectroscopic information on rotational temperatures was valuable for ground-based studies of the energy of precipitation.

Several workers (e.g. Romick et al., 1978; Vallance Jones et al., 1987; Koehler et al., 1981; Holma et al., 2000, 2003) used photometer channels with carefully selected narrow band interference filters, to measure the P and R branches of the N_2^+ 1NG (0,1) band. The ratio of the intensities of these channels gives an estimate of the variation in the shape of the rotational band, and thus of the neutral temperature. A more accurate measure of the shape of the rotational band is obtained with scanning spectrometers or imaging spectrographs. By fitting such measurements to synthetic spectra, the temperature of the emitting ions can be obtained, and hence the height of the emission region can be estimated from the neutral temperature profile, with similar assumptions mentioned above.

Henriksen et al. (1987) addressed the question of whether variations in neutral temperature could be caused by the changing height of the emission region, or by local heating. They used a 1 m Ebert-Fastie spectrometer to measure the N_2^+ 1NG (0,3) band and four O_2^+ 1NG bands. Ratios of different emissions have also been used for many years to estimate the energy of precipitation by association with the height of the emitting regions (e.g. Rees and Luckey, 1974; Kaila, 1989). The intensity ratio of N_2^+ 1NG (0,3) to O_2^+ 1NG (1,0) is dependent on height; Henriksen et al. (1987) used this ratio to derive the height of the aurora. The result was compared with that obtained by fitting the shape of the rotational bands to obtain the neutral temperature. The results from both methods were similar, inferring that changes in temperature were caused by changes in the height of the aurora and not by heating.

Temporal variations in the incident electron spectrum can be inferred from incoherent radar measurements in the magnetic zenith. Vallance Jones et al. (1987) compared such estimates of the average energy with those derived from optical emissions at Sondre Stromfjord, Greenland. Two optical methods were used: the intensity ratio I(6300)/I(4278) and also rotational temperatures derived from two photometer channels in the P and R branches of the N_2^+ 1NG (0,1) band. All three estimates gave similar results for the average primary electron energy. These authors used the results to validate a theoretical model of ion chemistry and optical emissions in the aurora. They calculated electron density height profiles from ionisation rate profiles, which were estimated from optical emissions (primary energies from N_2^+ rotational temperatures and total energy flux from I(4278)), and found a good agreement with the radar measurements.

The spectral signatures of the aurora contain information about the energy distribution of precipitating particles, and the state of the high altitude atmosphere. Theoretical models and synthetic spectra can be used to deduce much of this information. Higher spectral resolution gives more accurate results, allowing the clear separation of the rotational lines in the P and R branches, as long as there is sufficient signal in the wavelength region. The present work combines such high spectral resolution (0.08 nm) measurements from an imaging spectrograph viewing the magnetic zenith with narrow angle camera images, incoherent scatter radar measurements and an ion chemistry model of the auroral ionosphere. Analysis of spectral measurements of the N_2^+ 1NG (0,2) band (470.9 nm) has been performed with particular attention to the errors when fitting the measured spectra to synthetic spectra. This molecular band provides significant line intensities free of any contamination and overlapping from neighbouring bands. The present work highlights the importance of estimating the correct background to be subtracted from the emissions, as well as the effect that small deviations in wavelength calibration can have on the results.

2   Experimental details

The Spectrographic Imaging Facility (SIF) is a platform of optical instruments (University of Southampton and University College London), which is located in Nordlysstasjonen on Svalbard at geographic 78.2 N and 15.8 E. The main instrument, the High Throughput Imaging Echelle Spectrograph (HiTIES), is well documented (Chakrabarti et al., 2001; McWhirter et al., 2003; Lanchester et al., 2003). It was designed to measure several selected emissions simultaneously with high spectral and temporal resolution. The field of view is a narrow slit of length 8° centered on the magnetic zenith. Light is collimated, diffracted by a reflection echelon grating, and re-imaged onto the detector. High diffraction orders close to the blaze angle of the grating are used, which gives high spectral resolution and high throughput. The overlapping diffraction orders are separated by a mosaic of interference filters. The mosaic design determines the spectral and spatial coverage of the instrument. For the observations described here, a three panel mosaic was used, with spectral intervals for H_β, N_2^+ 1N bands 463.5–466.0 nm and 469.0–471.5 nm, and with all panels covering the 8° slit length. The detector used during these observations was the Microchannel Intensified CCD (Fordham et al., 1991). It is a photon counting detector, with very low dark count rate and no read-out noise. The spectral resolution of the spectrograph is determined by the slit width, which requires a compromise with the amount of light that enters the instrument. In these observations the resolution is 0.08 nm for the FWHM instrument function. Typical integration times are 10–60 s. Measurements can be integrated over different sections of the meridian slit as required. In the present measurements, time resolution of 30 s was used with readout time of 2 s, and integration over the slit was performed in steps of 1°.

The platform housed two photometer channels at the wavelengths of the H_β line near 486.1 nm, and of the N_2^+ 1N (1,3) band at 465.2 nm. A narrow angle camera measured the emissions in a field of view of 12° by 16° in the magnetic zenith. A short wavelength cut-off filter (645 nm) was used to eliminate the forbidden emissions from atomic oxygen, and to allow the prompt emission of N_2^+ (Meinel) and N_2 1PG bands to be imaged.

The European Incoherent Scatter (EISCAT) Svalbard Radar (ESR) is situated 7 km from Nordlysstasjonen on Svalbard. The data used here were taken with the TAU0 experiment. This is an alternating code experiment with two 960 μs pulses (15×64 s). The range separation of the samples is 2.4 km, but adjacent samples are not completely independent. The range covered is from below 100 km in the E region to the topside at 1000 km. The integration time in TAU0 is 12.8 s. However, the basic quantum is the time taken to transmit and receive the 64 repetitions of the modulation scheme needed to decode the alternating code, which is 640 ms. The integration time can be reduced to any multiple of this figure, with the aim of using the highest time resolution possible, depending on signal to noise ratio. An integration time of 6.4 s was used in the experiment. In order to increase the signal to noise pre-analysis integration of 32 s was used in the present work, which corresponds to the resolution of the spectrograph for these events.

3 Theory

Intensity calculations of the N_2^+ 1NG band spectra, which is a transition between two electronic states of N_2^+, are well documented (e.g. Herzberg, 1950; Degen, 1977). The energy of the molecule has terms corresponding to the vibrational and rotational degrees of freedom in addition to the energy of the electron states and can be acquired with harmonic oscillator and rigid rotor models in the following equation:

$$\overline{\epsilon}_{n,j} = \left(n + \frac{1}{2}\right)\overline{\omega} + \overline{B}_n J(J+1) \tag{1}$$

where

$$\overline{\omega} = \left(\frac{1}{2c\pi}\right)\sqrt{\frac{\kappa}{\mu}}, \quad \overline{B}_n = \frac{h}{8I_n c\pi^2} = \overline{B}_e - a\left(n + \frac{1}{2}\right) \tag{2}$$

n is the vibrational quantum number, $\overline{\omega}$ is the classical vibrational frequency of the bond i.e. band origin, κ is the bond strength, μ is the reduced mass, h is Planck's constant, c velocity of light, I is the moment of inertia of the system about its axis of rotation, J is the rotational quantum number, $\overline{B}_n$ is a rotational constant, $\overline{B}_e$ is the rotational term corresponding to the equilibrium bond length and a is the vibration-rotation interaction constant. Notation is in wavenumber. The sets of spectral lines forming within a vibrational band are known as the P ($\Delta J = -1$) and R ($\Delta J = +1$) branches in the $\Sigma-\Sigma$ state transitions. No Q-branch forms because the molecule has

no unpaired electrons. For $\overline{B}'_n > \overline{B}''_n$ the band head forms in the P-branch, as in the transition in our study, and in the opposite case in the R-branch. Band head by definition is the wavelength where the Fortrat parabola has a turning point. By standard notation, single prime corresponds to a vibrational level in a higher energy electronic state than double prime. Using the appropriate selection rules the positions of the vibration-rotation lines are predicted to lie at wavenumbers given by

$$\overline{\nu}_P = \overline{\omega} - (\overline{B}'_n + \overline{B}''_n)J'' + (\overline{B}'_n - \overline{B}''_n)J''^2 \tag{3}$$

$$\overline{\nu}_R = \overline{\omega} + 2\overline{B}'_n + (3\overline{B}'_n - \overline{B}''_n)J'' + (\overline{B}'_n - \overline{B}''_n)J''^2 \tag{4}$$

The rotational quantum number here corresponds to the vibrational state in the lower electronic state. The relation between wave number in air and vacuum has been applied from Morton (1991). The emission intensity distribution of these rotational lines follows the Maxwell-Boltzmann distribution law multiplied by a degeneracy factor $2J+1=J'+J''+1$, and becomes

$$I_{em} = \frac{C_{em}\overline{\nu}^4}{Q_r}(J' + J'' + 1)e^{-\overline{B}_{N2}J'(J'+1)hc/kT_r} \tag{5}$$

where C_{em} (for emission) is a constant depending on the total number of molecules in the initial vibrational level and change of dipole moment. Q_r is the rotational state sum, B_{N2} is the rotational constant in the neutral N_2 ground state, T_r is the rotational temperature and k is the Boltzmann constant. For a given band, it follows that the relative intensities of a rotation vibration band are given by

$$I_P \propto \overline{\nu}_P^4(2J)d_n e^{-\overline{B}_{N2}(J-1)Jhc/kT_r} \tag{6}$$

$$I_R \propto \overline{\nu}_R^4(2J + 2)d_n e^{-\overline{B}_{N2}(J+1)(J+2)hc/kT_r} \tag{7}$$

where d_n is the statistical weight for nuclear spin, which introduces an intensity alternation of neighbouring rotational lines. It follows from the selection rule $J'-J=\pm1$ that the even rotational number energy levels of N_2 X can only combine with the odd energy levels of N_2^+ X and that the transitions can only connect with rotational levels of equal nuclear spin degeneracy. This results in molecular nitrogen bands having an intensity ratio of 2:1 between even and odd numbers of rotational quantum number. Molecular constants for the modelling of synthetic spectra of molecular nitrogen bands can be found in Lofthus and Krupenie (1977). A typical modelled rotational structure of the N_2^+ 1NG (0,2) band can be seen in Fig. 1. The behaviour of a typical Fortrat parabola that is expected on the basis of Eqs. (3) and (4) is observed. Synthetic line spectra are convolved with a triangular instrument function of FWHM of 0.08 nm to acquire a theoretical convolved intensity as shown in Fig. 2 for the recorded HiTIES wavelength range 468.5–471.5 nm.
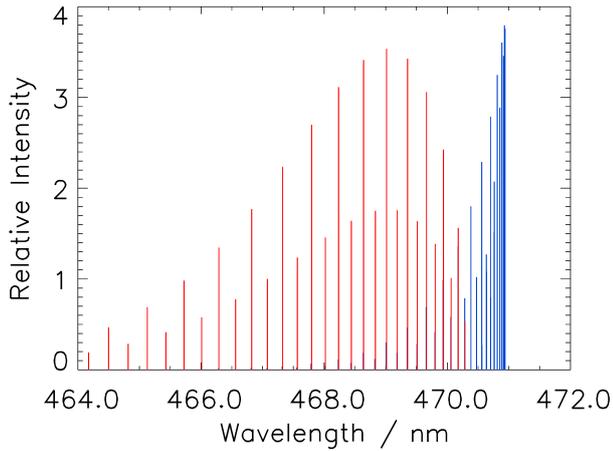
Fig. 1. Relative rotational intensities of P-branch (blue) and R-branch (red) of N_2^+ 1NG (0,2) synthetic spectra at 700 K. The band head forms in the P branch since $\overline{B}' > \overline{B}''$.
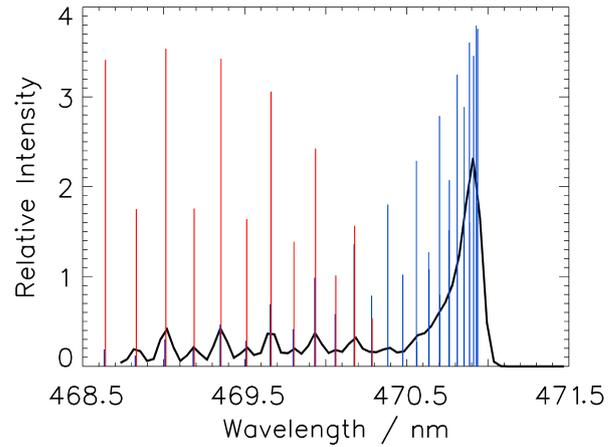
Fig. 2. Relative synthetic convolved spectra (black) superimposed on the synthetic rotational P- (blue) and R- (red) branches within the recorded wavelength interval of N_2^+ 1NG (0,2) in HiTIES.

4 Data analysis

The rotational temperature distribution of neutral N_2 is in thermal equilibrium with the surrounding species. Electron impact excitation from neutral N_2 X to N_2^+ B preserves the distribution between the rotational levels so that for the ions $T_r = T_n$, where T_n is the neutral temperature. Therefore it is assumed that measurements of the N_2^+ first negative band structure yields the neutral temperature of the emitting species.

The χ^2 statistic (Squires, 2001) is used to fit the observed profile and theoretical curve, where both scale factor and background are variable. This is given by

$$\chi^2 = \sum_{i=1}^{N} \left(\frac{e_i - \beta - \alpha t_i(T_r)}{\sigma_i} \right)^2 \tag{8}$$

where the e_i represent observed spectral intensities, β the background level, α the scale factor of the theoretical convolved line intensities t_i, T_r the rotational temperature, σ the standard deviation of the measured intensities and N the number of independent data points.

χ^2 is minimised with respect to α, β and T_r. Since the expression is a quadratic in α and β, this leads to the linear equations

$$\alpha = \frac{\sum e_i t_i(T_r) - \sum e_i \sum t_i(T_r)}{\sum t_i^2(T_r) - \sum t_i(T_r) \sum t_i(T_r)} \tag{9}$$

$$\beta = \sum e_i - \frac{\sum e_i t_i(T_r) - \sum e_i \sum t_i(T_r)}{\sum t_i^2(T_r) - \sum t_i(T_r) \sum t_i(T_r)} \sum t_i(T_r) \tag{10}$$

Minimisation of χ^2 is performed by plotting χ^2 with respect to T_r. Some typical curves are shown later in Fig. 10. If there is no aurora in the field of view then there may be no parabolic minimum in χ^2. In order to estimate the magnitude of the errors, the accuracy of the spectrograph allows us to assume the data points along the wavelength scale are statistically independent, so that the number of independent data points is simply the wavelength range divided by the spectrograph resolution.

It is not practical to measure σ, so the following argument is used to estimate the error ΔT_r in T_r. Assuming that the expected value of χ^2 from N independent measurements is equal to N allows an estimate of σ^2 to be made. If T_r is changed from $T_{r\text{minimum}}$ by one standard deviation ΔT_r, χ^2 should increase by unity. So for any constant σ

$$\chi^2(T_{r\text{minimum}} + \Delta T_r) = \frac{N+1}{N} \chi^2(T_{r\text{minimum}}) \tag{11}$$

The most dynamic aspect of the rotational spectrum as a function of temperature is the intensity at the band origin at 470.5 nm with respect to the intensity at the band head at 470.9 nm. The variability of this ratio is shown in Fig. 3. At $T_r < 500$ K the P-branch is mostly situated at the band head and the band origin is void of any rotational lines from the R-branch. Above this temperature the P-branch starts to spread beyond the band origin and overlap with the R-branch as seen in Fig. 1. A single temperature is fitted to a height integrated temperature profile and in order to make the fitting at the band origin agree with the overall χ^2 fit the relative standard deviation used is made dependent on wavelength.

As a consequence of the narrow rectangular slit at the input of the spectrograph, the CCD image is curved in the magnetic north-south direction (Chakrabarti et al., 2001). This is due to off-axis diffraction, the magnitude of which is wavelength dependent and means that the measured rotational lines are shifted on the wavelength scale along the magnetic meridian. A polynomial function was therefore applied to straighten
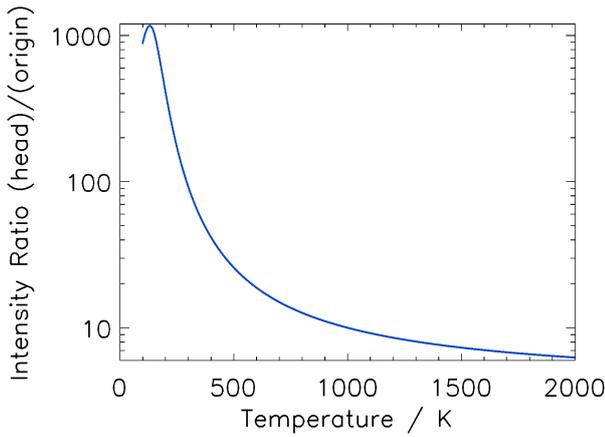
Fig. 3. Variation of the ratio of the intensity at the band head (470.9 nm) to the intensity at the band origin (470.5 nm) as a function of temperature.
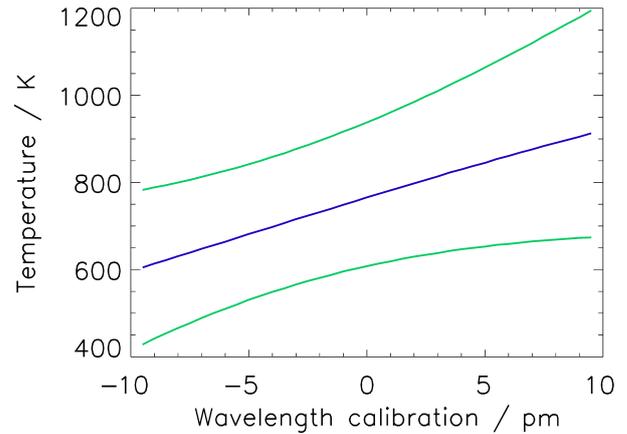
Fig. 4. The effect of wavelength calibration on best fitted temperature (blue) and error range (green) during a typical auroral event. Wavelength scale is in picometers.

the image. Because of the importance to match the synthetic spectra to the high resolution data accurately, fine wavelength calibration was also verified. To do this the pre-convolution theoretical spectrum was shifted with respect to the observed data. With the instrument function this will directly affect the shape of the convolved theoretical band. As a result, it can be seen in Fig. 4 that shifts of only 0.005 nm can lead to changes in temperature of the order of 100 K.

Measurements from the N_2^+ 1N(1,3) band are also used as an additional source of information. This wavelength range of the HiTIES mosaic filter includes the lines of the multiplet O^+ (^4P-$^4D^0$), which blend with the N_2^+ 1N(1,3) band, and are of comparable strength. An example of a measured spectrum from the spectrograph which includes both emissions, and a convolved theoretical spectrum of the nitrogen band is shown in Fig. 5. The relative intensity of the O^+ lines and N_2^+ bands is directly related to the energy of the incoming electron distribution (Ivchenko et al., 2004).

More supporting observations are electron density height profiles from the Eiscat Svalbard Radar (ESR). These are combined with an auroral model which provides a method of estimating the energy flux and peak energy of the incident electrons. It uses a one-dimensional electron transport code (Lummerzheim and Lilensten, 1994) and ion-chemistry equations (see Appendix in Lanchester et al., 2001). For the present data a simple method is used to fit the radar measurements to model height profiles of ionisation rates. However, the method shows clearly that the real energy spectrum of precipitating electrons is a much more complicated combination of several shapes, especially at time resolution of 30 s.

A flow diagram of the experimental approach is given in Fig. 6, following a similar system described in Vallance Jones et al. (1987). The spectrographic optical data provide the intensity of the two nitrogen bands (1,3) and (0,2). The
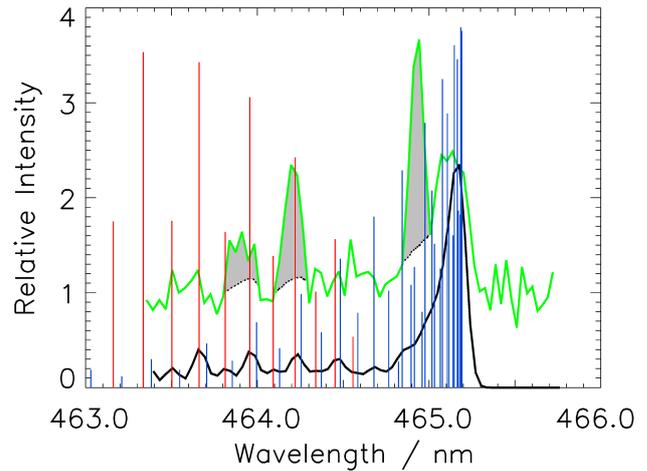
Fig. 5. Theoretical relative intensities of N_2^+ 1NG (1,3) P-branch (blue) and R-branch (red) with superimposed theoretical convolved intensities (black) and measured spectrographic profile (green) lifted up in the vertical scale, in which the three O^+(^4P-$^4D^O$) lines are clearly visible and marked grey.

latter is used to give a single, height integrated rotational temperature, which is then combined with the MSIS neutral temperature as a function of height, $T_n(h)$, to give an estimate of the height of the emissions. Thus the average energy $\langle E \rangle$ of the precipitating electrons can be estimated. The intensity of the oxygen lines found within the wavelength range of the N_2^+ 1N(1,3) band relative to the intensity of the nitrogen bands is an additional route to the average energy. The radar measurements give height profiles of electron densities, ionisation rate profiles, and thus an energy distribution function $\phi(E)$ and an estimate of the average energy. The height
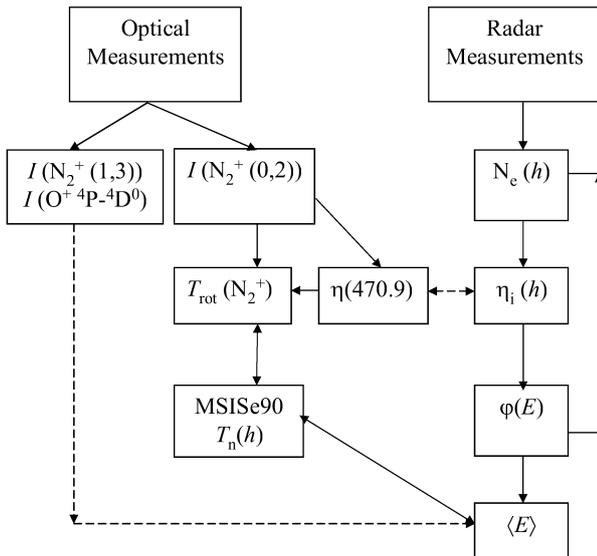
Fig. 6. Schematic diagram showing measured and modelled quantities starting from optical and radar input. Arrows show the possible paths linking the two.

Fig. 7. Electron precipitation events between 18:30–19:25 UT on 14 January 2002, measured with HiTIES: (first panel) N_2^+ 1NG (1,3) (465.2 nm) and $O^+(^4P-^4D^O)$ lines, (second panel) H_β (486.1 nm), (third panel) N_2^+ 1NG (0,2) (470.9 nm).

integrated production of 470.9 nm emission can be calculated by the model and compared with that measured, to complete the cycle. The last step will be done in future studies when more data sets at higher time resolution will be available. The present work is primarily to report the full details of the method for obtaining rotational temperatures from high resolution spectral data.

5   Results

5.1   Magnetic zenith

Strong electron precipitation was observed over Svalbard on 14 January 2002. An overview of the events analysed in this work is shown in Fig. 7, which is a time series of the spectrographic measurements over an hour from 18:30 UT. The top panel is N_2^+ 1NG (1,3) with band head at 465.2 nm. This includes the $O^+(^4P-^4D^0)$ lines, which have been reported in Ivchenko et al. (2004). The middle panel contains the Balmer H_β line; in the chosen interval there is a faint unshifted line at 486.1 nm from geocoronal hydrogen, and background Vegard-Kaplan band at the times of electron precipitation. This confirms that there is no significant Doppler shifted H_β, and therefore no proton precipitation during these events. The third panel is the N_2^+ 1NG (0,2) with band head at 470.9 nm. Arrows mark the times of three main events used for the temperature analysis at around 18:42 UT, 18:46 UT and 19:13 UT.

The radar (ESR) data from the same interval are shown in Fig. 8. The arrows again mark the events at 18:42 UT,

18:46 UT and 19:13 UT. The top panel shows that there is a strong increase in ion temperature preceding the first of these intervals, indicating the presence of electric fields in the region in advance of the auroral activity. There is also a large increase in electron temperature (panel 2) accompanying the event at 18:42 UT, and again to a lesser extent at 18:46 UT, but not at 19:13 UT. The F-region electron density in panel 3 is variable throughout the hour and could be the result of ionisation moving into the region across the polar cap, or soft precipitation causing ionisation at these heights. The precipitation that produces the auroral signatures is seen at the lowest heights in panel 3. These E region densities have been reproduced in panel 4 to show the differences in the distribution of ionisation in the chosen events over the height range 90–210 km.

The fitted N_2^+ 1NG (0,2) band for the chosen intervals are shown in Fig. 9. Frames from the auroral imager demonstrate the type of aurora that was in the field of view during the spectrographic and radar measurements are shown on the right. The spectral profiles are taken from 1° of the slit in the magnetic zenith and integrated over 30 s. The auroral image, on the other hand, is one frame lasting only a fraction of a second. In the first event, starting at 18:42:22 UT, the aurora was almost totally made up of rays, sometimes in rayed arc formation. In the second example shown (part of the same event), starting at 18:43:27 UT, the rayed arc is more evident with rays still dominating the aurora. In the third example (second event), starting at 18:46:13 UT, another auroral arc moved from the north into the field of view. This arc is without rayed structure, and has a curl forming along its length. The arc moved from the north (bottom) into the region of

the magnetic zenith without fully entering the radar beam. (Note that the radar beam is in the southern region of the slit.) Temperature analysis was successfully performed, both in the zenith position and along the slit to the north, discussed below. Comparison with radar data is used only as a source of background ionisation in this event. In the final event, starting at 19:13:19 UT, the aurora was very different in nature. Diffuse forms moved across the field of view, with dark lanes appearing at times. All of the above features are difficult to represent in still images.

The χ^2 fitted curves for the three distinct auroral events are shown in Fig. 10. The minimum of the parabola represents the best fit temperature. A wider parabola indicates uncertainty in T_r which can be due to random errors in the data and systematic errors due to a wider emission altitude range. The temperatures resulting from these fits, with their errors, are given at the top of each panel in Fig. 9 and in Table 1. At 18:42 UT and the subsequent interval shown in Fig. 9 one minute later, the aurora was dominated by rayed arcs, and the temperature was the highest value (800 K and 779 K, respectively). At 18:46 UT the aurora was in the form of a curling arc, with a lower temperature of 754 K in the zenith, which contained the highest part of the arc. Its lower border remained to the north of the zenith. This event is the best example of when the temperature from along the meridian slit is valuable. It is discussed further in Sect. 5.3. At 19:13 UT, during diffuse aurora, the temperature was at its lowest in the zenith (646 K).

The next stage of this analysis involves a simple application of a one-dimensional auroral model developed for the purpose of estimating energy fluxes and peak energies in electron precipitation regions (Palmer, 1995). In this method, an ionisation rate profile inferred from radar data is matched against model ionisation rate profiles, both Maxwellian and Gaussian (10% width), computed with a neutral atmosphere appropriate for the given position and date. This method provides an estimate of the main contributor to the energy spectrum. It is clear from previous work (Lanchester et al., 1997) and from this present analysis with relatively long integration times that the input spectrum is invariably much more complex, and is usually a mixture of more than one simple distribution. This has implications for the present results.

Two examples are shown in Fig. 11 of the fitted ionisation rate profiles. The EISCAT electron densities have been converted to ionisation rate profiles, assuming a constant recombination rate coefficient. Although this is an approximation, it allows a good estimate of the peak energy of the precipitating flux. It also gives reasonable limits for the energy flux. In the first panel of Fig. 11 at 18:42 UT, the radar profiles are fitted well by a Maxwellian distribution at the lowest heights, with peak energy of about 1 keV. However, above 170 km the measured profile is not fitted. Another distribution is present at these heights. In the second panel, at 19:13 UT, both a Maxwellian and a Gaussian have been fitted, showing that the real spectrum is a mixture of more
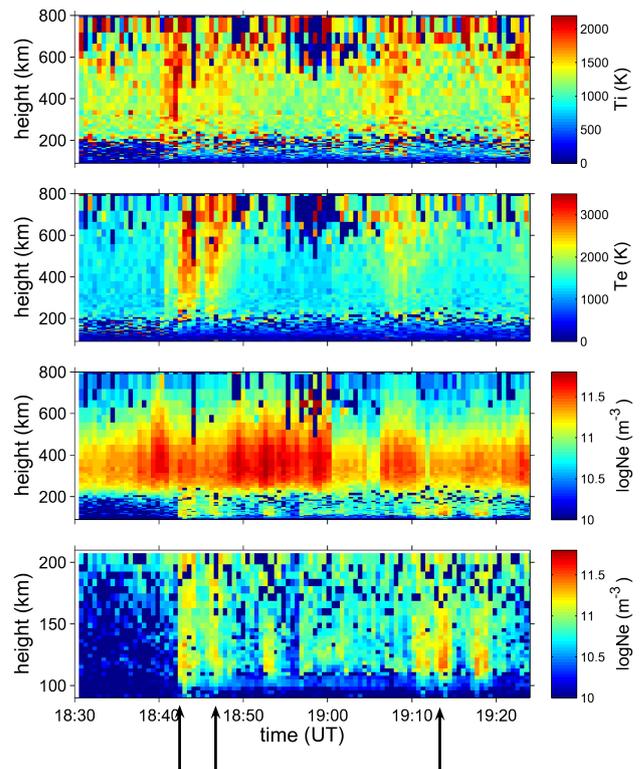
Fig. 8. Overview of radar measurements between 18:30–19:25 UT on 14 January 2002. Height profiles of ion temperature (first panel), electron temperature (second panel), F-region electron density (third panel) and E-region electron density (fourth panel).

than one distribution. The peak energy from the Gaussian is 3.4 keV. Again, there is another distribution this time above 140 km, but not as marked as in the previous example. This difference can be seen in Fig. 8, comparing the times marked with the first and third arrows. There is a clear region of increased electron density above 170 km at 18:42 UT, and a less intense increase at around 150 km at 19:13 UT. The peak energies inferred from the fitted profiles for three times shown in Fig. 9 are included in Table 1. The rayed aurora is associated with smaller values of energy of precipitation (maximum of 1 keV) and corresponds to larger neutral temperatures. As already noted, the curling arc of the second event was not fully measured by the radar at 18:46 UT and is not included in the zenith analysis. Larger values of precipitation energy (maximum of 3.4 keV) occurred during the diffuse aurora, which corresponds to the smallest neutral temperatures in the zenith.

Estimates of the energy flux are also included in the table, although these are only a guide for comparison between events. The fits do not account for populations observed in the upper E region, which also means that the peak energy is representative of only one population. The average energy from neutral temperature will include contributions from all populations.
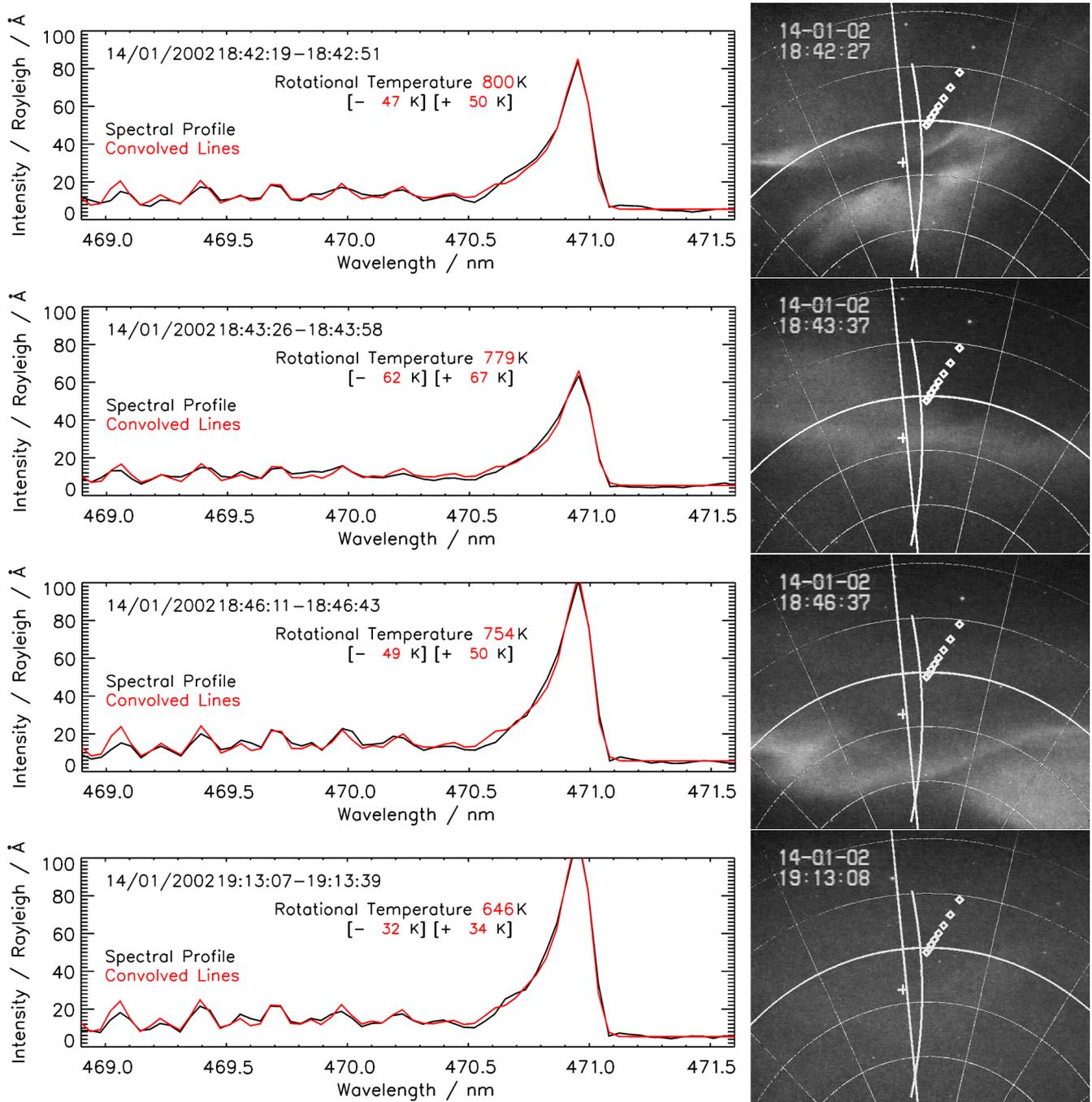
Fig. 9. (left)Spectral fits for aurora at 18:42 UT, 18:43 UT, 18:46 UT and 19:13 UT. Rotational temperature decreases from top (rays) to bottom (diffuse). (right) Images from the narrow angle auroral imager; the spectrograph slit position and the radar beam projected to heights 100–240 km with 20 km separation are shown in each image. South is at the top and east on the right.

As described in the flow diagram of Fig. 6, the two approaches taken above can be compared by estimating the energy of the precipitation from both optical and radar measurements. The MSISe90 atmospheric model for the 14 January 2002 has been used to convert the derived neutral temperatures to average heights of emission. The results are included in Table 1. The auroral model (Palmer, 1995) is again used to provide a value for the energy associated with maximum emission at the estimated heights. These are included in Table 1. In the first two intervals, Maxwellian distributions

Table 1. Summary of derived temperature, estimated energy distributions, and ratio of emissions $I(O^+)/I(N_2^+(0,2))$ at four chosen times, in different types of aurora.

time (UT)	type	T_n zenith (K)	height (km)	$\langle E \rangle$ optical (keV)	main $\varphi(E)$ radar	peak E, radar (keV)	energy flux, radar (mW m^2)	emission ratio $I(O/N)\times 100$
18:42	rays	800±50/47	156±6	0.5 (M)	Maxwellian	1.0	2.4	17.32
18:43	rayed arc	779±67/62	154±8	0.5 (M)	Maxwellian	1.0	4.0	
18:46	curled arc	754±50/49	150±5	1.2 (G)				6.90
19:13	diffuse	646±34/32	139±4	1.5 (G)	Gaussian	3.4	4.1	10.23

were used following the evidence from the radar observations. Monoenergetic beams of electrons approximated by a Gaussian distribution were used for the third event. This is of course a gross assumption, since the ionisation rate profiles clearly show that the real distributions must be much more complex, and in all cases lower energy populations were also present. However, the agreement between the energy from optical methods, and the peak energy from radar is reasonable. In all cases the peak energy is approximately double the optically derived energy. This is not a property of the Maxwellian or Gaussian shape assumed, but of the profile-integration included in the optical method, and not in the radar method.

5.2 Emission ratios

The events of 14 January 2002 during the same time interval have been used in a separate analysis by Ivchenko et al. (2004). The purpose of that work was to report observations of O^+ lines in electron aurora over Svalbard, and to use measurements of the brightness of these lines compared with the brightness of the N_2^+ 1N(0,2) band (see Fig. 5) to estimate the cross section for production of the multiplet in electron collisions. That work showed how the variation of the ratio of the brightnesses is linked with the type of aurora, and hence with the energy of precipitation, and the height at which the emissions are maximum. The most common value of the ratio of these emission brightnesses was found to be about 0.1. In the first event here, the predominance of O^+ lines over the N_2^+ is very clear with a ratio 0.17, and confirms the observation that the O^+ emissions are associated with low energy precipitation within rayed aurora. The second event with the curling arc (well-measured by the spectrograph but not the radar) gives a ratio well below 0.1, when the N_2^+ emission dominates. In the third event the ratio is at a normal level close to 0.1. The temperature results from the same events are consistent with the above interpretation, and provide the dashed link in the flow diagram of Fig. 6.

5.3 Along the meridian slit

The original spectrograph design was intended to provide information about auroral variations along the magnetic merid-
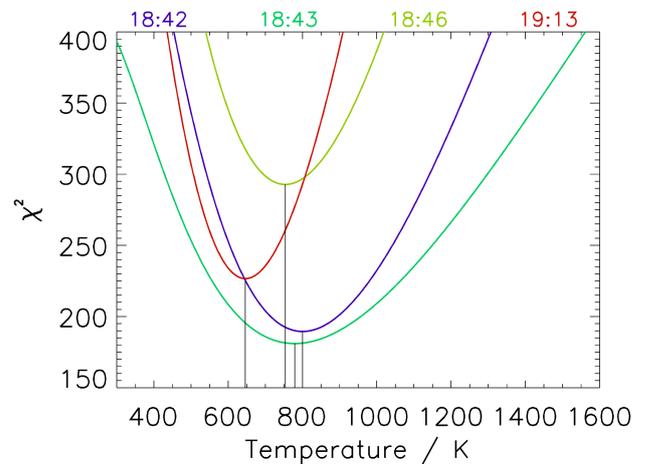
Fig. 10. χ^2 fit curves for the four intervals of electron precipitation at 18:42 UT, 18:43 UT, 18:46 UT and 19:13 UT on 14 January 2002.

ian centred on the magnetic zenith. At the time resolution of the present data of 30 s, the variations in the aurora must be considered carefully. As an extra check on the validity of the zenith results, the variation of derived temperatures across the meridian slit of the spectrograph has been examined in all of the above events. In the first event, the aurora was consistently rayed, which can be approximated by a distribution along the slit with lower energies nearer the middle. In the second event, the curling arc was seen to reach the zenith, and stay with its lower border to the north of the zenith for most of the integration time. In this example it was advantageous that a measurement of temperature could be made at the maximum intensity in the arc, with less contamination from the integrated profile. The third event was made up of diffuse aurora which mostly filled the slit, with the exception of dark lanes for short intervals.

The geometry of the optical instruments is shown in Fig. 12 with three possible arc positions marked. Arc A corresponds to the results of Sect. 5.1, where the zenith measurements are necessarily an integration over all heights in the aurora that enters this region; the derived temperatures

18:42.25 UT

19:13.19 UT
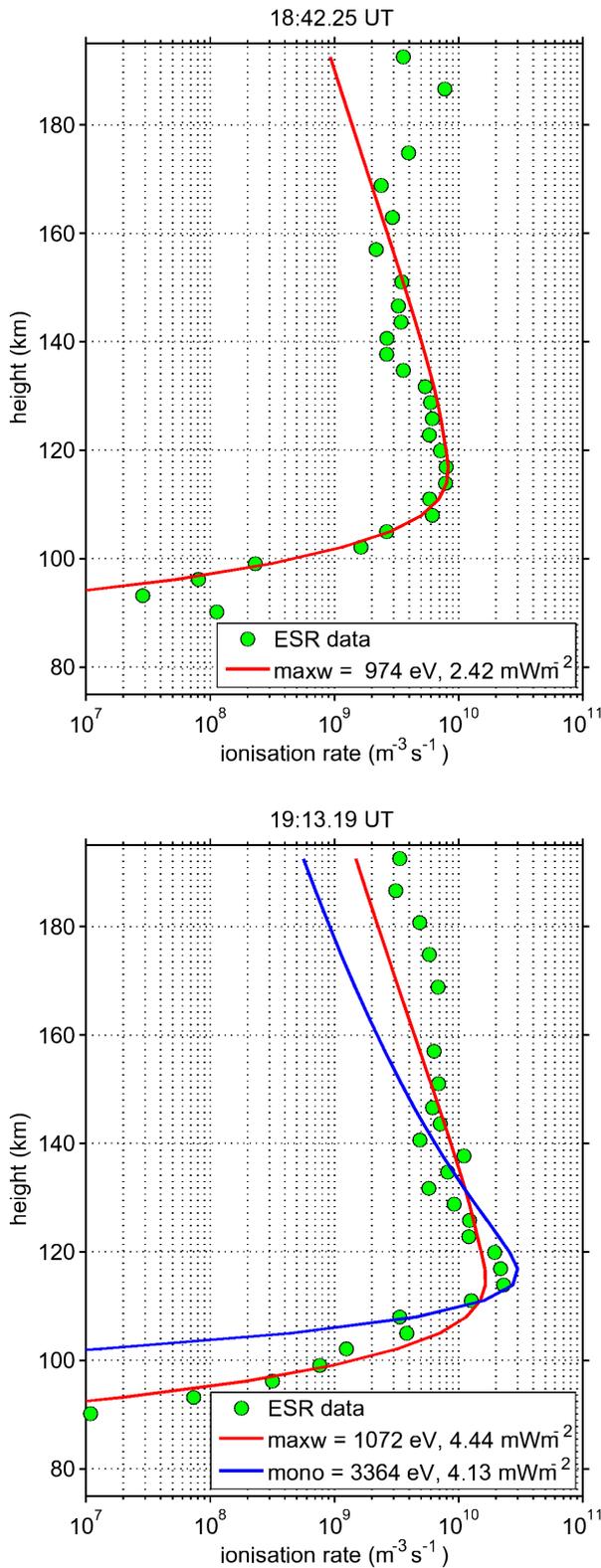
Fig. 11. Ionisation rate profiles from radar, and fitted profiles from model for rayed aurora (18:42 UT) and diffuse aurora (19:13 UT).
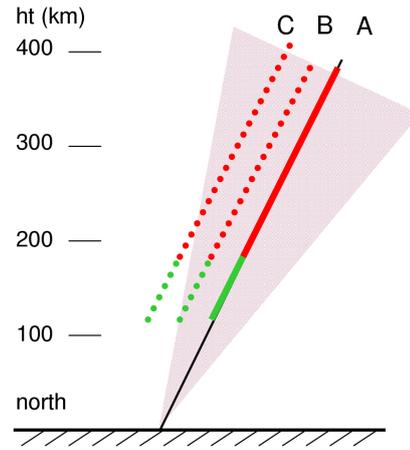
Fig. 12. Schematic diagram (not to scale) of the geometry of the HiTIES spectrograph with auroral arcs in three positions in the field of view. The shaded area represents the 8° slit along the magnetic meridian. Arc at position A corresponds to the magnetic zenith.

are therefore dominated by the type of aurora that is present. In order to estimate changes in the temperature associated with different heights within an auroral feature, ideally an arc must stay in a position such as that marked B for the integration interval. In such a case, the region to the edge of the slit measures the lower part of the arc (lower temperatures) with temperature increasing towards the zenith point. Another possible situation is described by an arc in position C, which has its lower border out of the field of view of the slit, but its highest part is measured on the edge of the slit. This figure also demonstrates how each elevation angle (other than the magnetic zenith) may contain contributions from more than one auroral form. The data have been interpreted with careful consideration of all these possibilities.

The main problem with this approach is the need for temporal integration of the spectrograph profiles, which in the present data was 30 s, necessary for the detector in use at the time. From the video sequences throughout the events described it is clear that the aurora often varied on much shorter time scales than this, resulting in some spatial and temporal averaging. Given this caviat, the temperature fits for the data in the three events are consistent with the geometry of the aurora measured, and with the zenith measurements.

Each of the three events is represented in Fig. 13. The left hand panels in each are taken from the narrow angle camera, and show the variations in intensity in the region corresponding to the spectrograph slit for the integration interval of 30 s, shown as the time axis. The right hand panels are temperature fits in 1° slices. (The zenith value in each case is the temperature given in Table 1.). The spectrograph data from the N_2^+ 1NG (1,3) filter with band head at 465.2 nm have been used as a diagnostic for the varying emissions along the slit. The $O^+(^4P\text{-}^4D^0)$ lines at 464.9 nm (the brightest), 464.2 nm

and 463.9 nm, produced by low energy precipitation, were measured with variable brightnesses in different regions of the slit in each event. In Fig. 14 two spectra have been chosen from different elevation angles, to show the different contributions of the $O^+(^4P-^4D^0)$ lines relative to the N_2^+ 1NG (1,3) band head. For the first event, starting at 18:42 UT oxygen lines dominate, and in particular at the position 1° north of the zenith, where the temperature is indeed even higher (850 K) than that in the zenith (800 K). The nitrogen band is stronger to the south of the zenith where the temperature decreases with angle of elevation, as given by aurora in position B in Fig. 12. This result agrees with the observation that the rays were distributed through this region and the brighter features were seen mostly in the southern half of the field of view. The second interval at 18:43 UT is a continuation of the same event of rayed arcs in the field of view. It gives a similar result, with maximum temperature of 800 K at the zenith position, decreasing to 600 K away from the zenith. This corresponds to a temporal integration producing an average temperature profile at each elevation angle. The intensity of the oxygen lines is above that of the nitrogen band over the whole slit.

In the second event at 18:46 UT, a curling arc approached from the north and only briefly moved into the zenith. Weaker aurora was seen for part of the interval just south of the zenith. The resulting temperature profile is in agreement with this finding, with lowest temperatures of 550 K at the northern edge, corresponding to the lower border of the arc, and highest temperatures in the zenith. This corresponds to an energy in the lower border of the arc of a few keV, originating from heights of 120 km, a very reasonable result for a curling bright arc (Rees, 1989). Figure 15 shows that the nitrogen band head dominates the spectral measurements on the northern side of the slit. South of the zenith in weaker aurora, the oxygen lines are slightly more prominent again.

Finally, the event at 19:13 UT is quite different in all respects. The aurora shows very little structure along the slit, as do the temperatures. In the southern half of the slit the temperatures do not reduce towards the edge and are all below 700 K. The zenith measurement of 650 K is in fact the lowest value, with an increase of nitrogen band here (not shown). The very low temperature at the northern edge appears to be associated with a sharp edge between diffuse aurora and a dark lane that moves across the field of view. Higher time resolution is needed to study such features.

6   Discussion

The fitting of measured nitrogen bands to convolved theoretical spectra as a function of temperature is the primary motivation for the present work. The analysis has been performed with particular attention to errors in the fit, with consideration for the assumptions inherent in noisy data. The inclusion of the background as an unknown parameter in the fitting
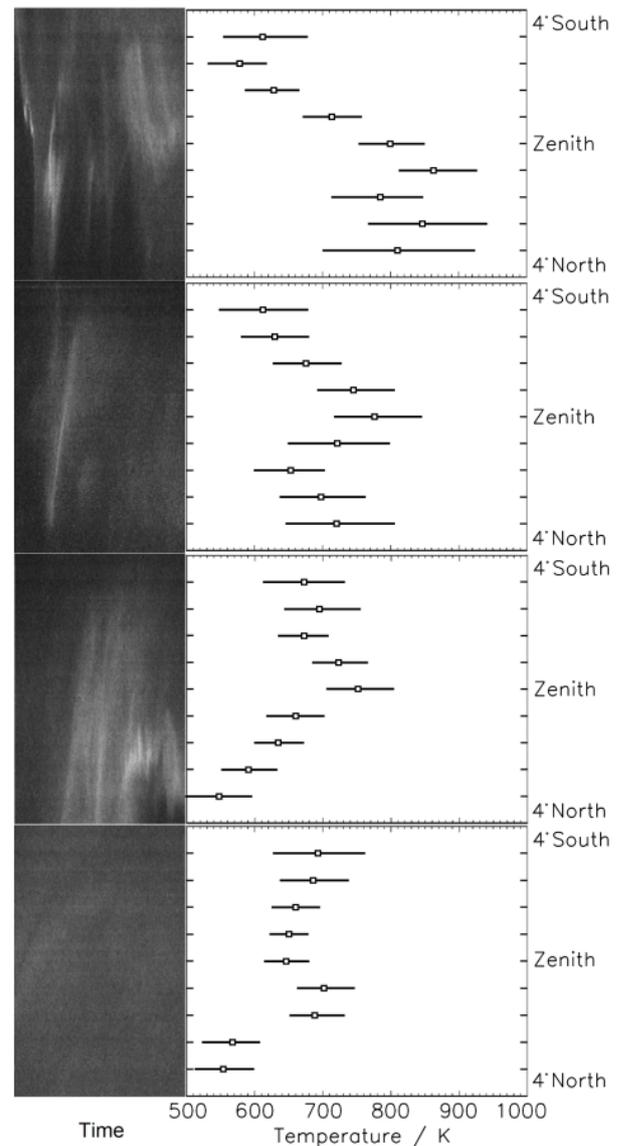
Fig. 13. From top to bottom at 18:42 UT, 18:43 UT, 18:46 UT and 19:13 UT: (left panels) intensity in slit measured by narrow angle camera over 30 s; (right panels) rotational temperatures in 1° steps along the HiTIES slit.

means that this is a dynamic process, and much more likely to produce accurate temperatures than the use of an average background value. The consistency of the resulting temperatures with our understanding of the physical processes in the auroral ionosphere gives confidence in the experiment.

The analysis has been performed for magnetic zenith profiles, as well as for measurements at small elevation angles away from the zenith which, with careful choice, represent measurements at different heights of an auroral form. The time resolution of the data is the limitation in such an analysis, and this has been taken into account in the events chosen.
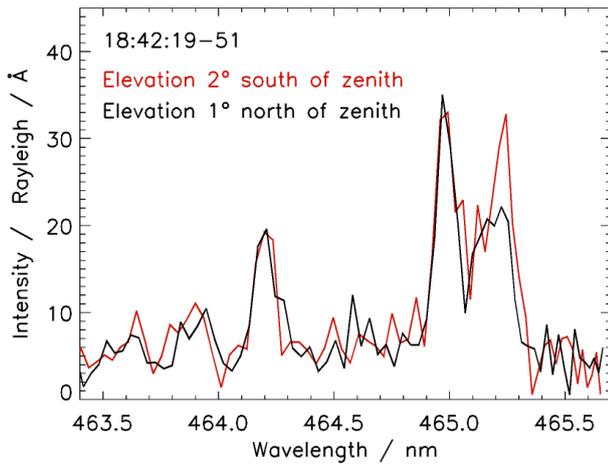
Fig. 14. Spectra from two elevation angles across the HiTIES slit at 18:42 UT, showing the relative change in intensity of the Oxygen lines with respect to the Nitrogen band head, corresponding to changes in the derived temperature seen in Fig. 13.
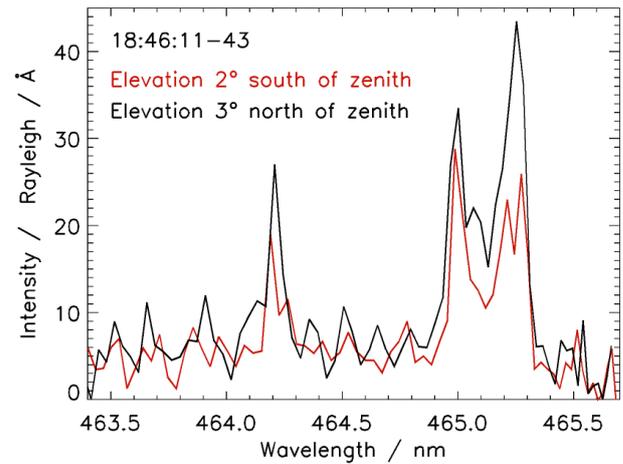
Fig. 15. Spectra from two elevation angles across the HiTIES slit at 18:46 UT, showing the dominance of the Nitrogen band head at elevation angle 3° north of zenith, corresponding to low values of derived temperature shown in Fig. 13.

Higher time resolution using a new detector will be used in future.

The spread in fitted temperatures between 500–900 K corresponds to a height range of approximately 120–170 km when compared with the MSIS atmospheric model. This is very close to the height range of emission maxima in aurora at the latitude of Svalbard. As can be seen from the table of results, the inferred average energies using the optical route are in good agreement with those derived from radar and modelling. The former gives energy estimates which are necessarily an average value, since they are derived from an integrated zenith measurement. The latter gives estimates of peak energy, derived from a height profile of ionisation rates. These peak energies are expected to be larger than the optical values, since they ignore the ionisation rate increases above the peak. In order to calculate a neutral temperature more accurately in the magnetic zenith, the analysis could be improved by fitting a height integrated temperature profile rather than a single temperature. This would compare more favorably with height integrated intensities derived from model and radar.

Interest in the chosen date and time interval stemmed from the results described in Ivchenko et al. (2004). In their work, O^+ lines were found to dominate the $N_2^+(1,3)$ band region at times of rayed aurora, and low energy precipitation. A very detailed analysis was made in that work of the intensity ratio $I(O^+)/I(N_2^+(0,2))$. The ratio is largest for the time of lowest energy, and highest temperature (18:42 UT). The lowest ratio is at the time of the curled arc (18:46 UT), when the N_2^+ bands were stronger. In this event, the measurements along the meridian are valuable. The temperature fits taken from north of the zenith confirm that the peak energy in this arc was several keV. For the final event with diffuse aurora

the $I(O^+)/I(N_2^+(0,2))$ ratio has the average value of 0.1. The ionisation rate profiles from the radar indeed show that the distribution is not a single Maxwellian nor the result of a monoenergetic beam, but a combination of both in the lower E region, and another broader distribution above 150 km.

The possible effect of changes to the temperature of electrons and ions can be considered from the radar data. Electron temperatures, T_e, were raised to values above 2000 K over a wide height range as seen in Fig. 8 at the time of the first event between 18:42 UT and 18:44 UT. T_e will increase from heating due to precipitation, but also from the presence of field-aligned currents through Ohmic heating (Lanchester et al., 2001; Zhu et al., 2001). The analysis of this event shows that there is an abundance of low energy electrons, with an increase in the ionisation rate profile above 170 km superimposed on the fitted Maxwellian. Low energy electrons are the main contributor to field-aligned current density. The measured increase in ion temperature immediately preceding this event also indicates the presence of strong currents, with horizontal electric fields and flows in the immediate region of the auroral precipitation (Lanchester et al., 1996; Zhu et al., 2001).

The absence of an increase in T_e in the diffuse aurora at 19:13 UT is also significant, suggesting that there are no strong field aligned currents, and not much heating from precipitation. Here the neutral temperature is lower, as a result of an increase in precipitation energy. The values of the energy flux throughout the interval 18:30–1930 UT calculated from the 1-D auroral model show very similar energy fluxes for the times with rays and with diffuse aurora (see Table 1). As found by Henriksen et al. (1987), the fact that the results obtained for the energy of precipitation from

optical and radar measurements are in good agreement implies that the changes in neutral temperature were caused by changes in the height of the emission region, and not on local heating. There is no evidence that the electron temperature increase has any direct effect on the neutral temperature measurements, although it corresponds with the time of greatest T_n. Further studies will be made to confirm this conclusion.

7   Conclusions

First results from spectrographic measurements at high spectral resolution provide neutral temperatures in the magnetic zenith and within auroral features close to the zenith. The analysis is more accurate than previous measurements, with particular attention paid to the errors associated with the background subtraction and wavelength calibration.

A clear trend in neutral temperature is found, with higher values for times of lower energy precipitation and vice versa. The events chosen contain times of very different auroral types, and clear differences in the neutral temperatures associated with them. The variation in neutral temperatures across the meridian slit was shown to be consistent the result from the zenith, with higher temperatures for regions at greater heights nearer the zenith, and lower temperatures in the lower borders of one arc in particular. An increasing temperature profile along the slit, from the edge of the slit to the zenith, was found during the time of rayed aurora, on both sides of the zenith.

Although there were large variations in the electron temperatures measured by the radar, the results suggest that there was no direct effect on the neutral temperature. Rather it is considered that the increases in both T_e and T_n at the time of rayed aurora were both associated with low energy precipitation. While the measured T_e increase is an actual temperature increase, the measured T_n increase results from the change of emission altitude in this type of precipitation.

References

Brandy, J. H.: Rotational temperatures of the auroral 3914 Å nitrogen band vs. height at Churchill, Manitoba, Can. J. Phys., 31, 1793–1797, 1964.

Chakrabarti, S., Pallamraju, D., Baumgardner, J., and Vaillancourt, J.: HiTIES: A High Throughput Imaging Echelle Spectrograph for ground-based visible airglow and auroral studies, J. Geophys. Res., 106, 30 337–30 348, 2001.

Degen, V.: Modeling of N_2^+ First Negative spectra excited by electron impact, J. Quant. Spectroscopic Radiat. Transfer, 18, 113–119, 1977.

Fordham, J. L., Bellis, J. G., Bone, D. A., and Norton, T. J.: MIC photon counting detector, in: Proc. SPIE, 1449, Electron Image Tubes and Image Intensifiers II, edited by: Csorba, I. P., 87-98, 1991.

Harang, L.: The Aurorae, Chapman and Hall Ltd., p. 83, 1951.

Hedin, A. E.: Extension of the MSIS thermosphere model into the middle and lower atmosphere, J. Geophys Res., 96, 1159–1172, 1991.

Henriksen, K., Veseth, L., Deehr, C. S, and Smith, R. W.: Neutral temperatures and emission height changes in an E-region aurora, Planet. Space Sci., 35, 1317–1321, 1987.

Herzberg, G.: Spectra of diatomic molecules, 2nd edition, edited by: van Nostrand, D., 1950.

Hilliard, R. L. and Shepherd, G. G.: Upper atmosphere temperatures from Doppler line widths, 4. A detailed study using the OI 5577 Å auroral and nightglow emissions, Planet. Space Sci., 14, 383–406, 1966.

Holma, H. A., Kaila, K. U., and Jussila, J. R. T.: Temperatures, emission heights and energies in discrete auroral forms, Phys. Chem. Earth (B), 25, 463–466, 2000.

Holma, H. A., Kaila, K. U., and Jussila, J. R. T.: Electron energy estimations in an auroral arc, Proc. 28th Ann. Europ. Meeting of Atmospheric Studies by Optical Methods, S.G.O. Publications 92, 105–108, 2003.

Hunten, D. M., Rawson, E. G., and Walker, J. K.: Rapid measurement of N_2^+ rotational temperatures in aurora, Can. J. Phys., 41, 258–270, 1963.

Ivchenko, N., Galand, M., Lanchester, B. S., Rees, M. H., Lummerzheim, D., Furniss, I., and Fordham, J.: Observation of $O^+(^4P\,-^4\,D^0)$ lines in proton aurora over Svalbard, Geophys. Res. Lett., 31, L10807, doi:10.1029/2003GL019313, 2004.

Kaila, K. U.: Determination of the energy of auroral electrons by the measurements of the emission ratio and altitude of aurorae, Planet. Space Sci., 37, 341–349, 1989.

Koehler, R. A., Shepherd, M. M., Shepherd, G. G., and Paulson, K. V.: Rotational temperature variation in pulsating auroras, Can. J. Phys., 59, 1143–1149, 1981, Ann. Geophys., 19, 643–648, 1981,
http://www.ann-geophys.net/19/643/1981/.

Lanchester, B. S., Kaila, K. U., and McCrea, I. W.: Relationship between large horizontal electric fields and auroral arc elements, J. Geophys. Res., 101, 5075–5084, 1996.

Lanchester, B. S., Rees, M. H., Lummerzheim, D., Otto, A., Frey, H. U., and Kaila, K. U.: Large fluxes of auroral electrons in filaments of 100 m width, J. Geophys. Res., 102, 9741–9748, 1997.

Lanchester, B. S., Rees, M. H., Lummerzheim, D., Otto, A., Sedgemore-Schulthess, K. J. F., Zhu, H., and McCrea, I. W.: Ohmic heating as evidence for strong field-aligned currents in filamentary aurora, J. Geophys. Res., 106, 1785–1794, 2001.

Lanchester, B. S., Rees, M. H., Robertson, S. C., Galand, M., Lummerzheim, D., Baumgardner, J., Mendillo, M., Furniss, I., and Aylward, A. D.: Proton and electron precipitation over Svalbard – first results from a new Imaging Spectrograph (HiTIES), Proc. 28th Ann. Europ. Meeting of Atmospheric Studies by Optical

Methods, S.G.O. Publications, 92, 33–36, 2003.

Lofthus, A. and Krupenie, P. H., The spectrum of molecular nitrogen, J. Phys. Chem. Ref. data, 6(1), 307 p., 1977.

Lummerzheim, D. and Lilensten, J.: Electron transport and energy degradation in the ionosphere: evaluation of the numerical solution, comparison with laboratory experiments and auroral observations, Ann. Geophys., 12, 1039–1051, 1994, http://www.ann-geophys.net/12/1039/1994/.

McWhirter, I., Furniss, I., Aylward, A. D., Lanchester, B. S., Rees, M. H., Robertson, S. C., Baumgardner, J., and Mendillo, M.: A new spectrograph platform for auroral studies in Svalbard, Proc. 28th Ann. Europ. Meeting of Atmospheric Studies by Optical Methods, S.G.O. Publications, 92, 73–76, 2003.

Miller, J. R. and Shepherd, G. G.: Auroral measurements using rocket-borne photometers, Ann. Geophys., 24, 305–312, 1968, http://www.ann-geophys.net/24/305/1968/.

Morton, D. C.: Atomic Data for Resonance Absorption Lines, Astrophys. J. suppl. S, 77, 119–202, 1991.

Palmer, J. R.: Plasma density variations in the aurora, PhD thesis, University of Southampton, 1995.

Rees, M. H. and Luckey, D.: Auroral electron energy derived from ratio of spectroscopic emissions 1. Model computations, J. Geophys. Res., 79, 5181–5186, 1974.

Rees, M. H.: Physics and chemistry of the upper atmosphere, Cambridge University Press, p. 41, 1989.

Romick, G. J., Degen, V., Stringer, W. J., and Henricksen, K.: The altitude profile of N_2^+ first negative rotational temperature in auroral arc, J. Geophys. Res., 83, 91–96, 1978.

Shepherd, G. G. and Eather, R. A.: On the determination of auroral electron energies and fluxes from optical spectral measurements, J. Geophys. Res., 81, 1407–1410, 1976.

Shepherd, G. G. and Hunten, D. M.: On the measurements of rotational temperature from unresolved auroral nitrogen bands, J. Atmos. Terr. Phys., 6, 328–335, 1955.

Squires, G. L.: Practical physics, Fourth Edition, Cambridge University Press, p. 176, 2001.

Vallance Jones, A., Gattinger, R. L., Shih, P., Meriwether, J. W., Wickwar, V. B., and Kelly, J.: Optical and radar characterization of a short-lived auroral event at high latitude, J. Geophys. Res., 92, 4575–4589, 1987.

Vegard, L.: Results of investigations of the auroral spectrum during the years 1921–1926, Geophys. Publ., 9(11), 1–71, 1932.

Zhu, H., Otto, A., Rees, M. H., Lanchester, B. S., and Lummerzheim, D.: Ionosphere-magnetosphere simulation of small scale structure and dynamics, J. Geophys. Res., 106, 1795–1806, 2001.

Zwick, H. H. and Shepherd, G. G.: Upper atmospheric temperatures from Doppler line widths -v. Auroral electron energy spectra deduced from the 5577 and 6300 Å atomic oxygen emissions, Planet. Space Sci., 21, 605–621, 1973.